Synthesis of palladium-rhodium bimetallic nanoparticles for formic acid dehydrogenation

Synthesis of Palladium-Rhodium bimetallic Nanoparticles for Formic Acid Dehydrogenation

Ilaria Barlocco,[a] Sofia Capelli,[a] Elisa Zanella,[a a] Xiaowei Chen,[b] Juan J. Delgado,[b] Alberto Roldan, [c] Nikolaos Dimitratos,[d,*] Alberto Villa [a,*]

a Dipartimento di Chimica, Università degli Studi di Milano, Milan, I-20133, Italy

b Departamento de Ciencia de los Materiales, Ingeniería Metalúrgica y Química Inorgánica, Facultad de Ciencias, Universidad de Cádiz, Campus Río San Pedro, Puerto Real (Cádiz), E-11510, Spain

c School of Chemistry, Cardiff University, Main Building, Park Place, CF10 3AT, Cardiff, United Kingdom

d Dipartimento di Chimica Industriale e dei Materiali, ALMA MATER STUDIORUM Università di Bologna, Viale Risorgimento 4, I-40136 Bologna

† In memory of Dangsheng Su who was a source of inspiration for us

*Corresponding authors

E-mail addresses: Alberto.Villa@unimi.it (A. Villa), Nikolaos.Dimitratos@unibo.it (N. Dimitratos)

Abstract

Herein, we report for the first time the synthesis of preformed bimetallic Pd-Rh nanoparticles with different Pd:Rh ratios (nominal molar ratio: 80-20, 60-40, 40-60, 20-80) and the corresponding Pd and Rh monometallic ones by sol immobilization using polyvinyl alcohol (PVA) as protecting agent and $NaBH_4$ as reducing agent, using carbon nanofibers with high graphitization degree (HHT) as the desired support. The synthesized catalysts were characterized by means of Transmission Electron Microscopy (TEM) and Inductively coupled plasma optical emission spectroscopy (ICP-OES). TEM shows that the average particle size of the Pd-Rh nanoparticles is the range of 3-4 nm, with the presence of few large agglomerated nanoparticles. For bimetallic catalysts, EDX-STEM analysis of individual nanoparticles demonstrated the presence of random-alloyed nanoparticles even in all cases Rh content is lower than the nominal one (calculated Pd:Rh molar ratio: 90-10, 69-31, 49-51, 40-60). The catalytic performance of the Pd-Rh catalysts was evaluated in the liquid phase dehydrogenation of formic acid to H_2. It was found that Pd-Rh molar ratio strongly influences the catalytic performance. Pd-rich catalysts were more active than Rh-rich ones, with the highest activity observed for Pd_{90}:Rh_{10} (1792 h^{-1}), whereas Pd_{69}:Rh_{31} (921 h^{-1}) resulted the most stable during recycling tests. Finally,

Pd_{90}:Rh_{10} was chosen as a representative sample for the liquid-phase hydrogenation of muconic acid using formic acid as hydrogen donor, showing good yield to adipic acid.

Introduction

Noble metals alloyed nanoparticles (NPs) are fundamental for several essential industrial processes. Although academia is switching its attention on cheaper and abundant transition metals, industries continue to employ noble metal-based catalysts due to their higher activity, stability and their well comprehended chemistry [1,2]. For these reasons a key challenge is to modify these catalysts, increasing their catalytic properties such as activity, selectivity and stability. In particular, palladium-based catalysts are widely employed in different types of heterogeneous catalytic reactions, such as hydrogenations [3] and oxidations [4,5].

The addition of a second metal to Pd (e.g. Au, Ag, Ni, etc) can tune the catalytic properties of the material, often enhancing activity, selectivity and stability of the catalyst due to the formation of new electronic states (ligand effect) combined with the strain of the lattice (steric effects) [6,7]. Rhodium also plays a fundamental role in many reactions such as the C-H activation [8]. The Pd-Rh system is barely studied. However, it was reported that alloying Rh to Pd it is possible to enhance the activity and stability of pure Pd in different reactions, including hydrogenation of cyclohexene [9], oxidation of o-phenylenediamine [10] and ethanol steam reforming [11]. The problem is that it is difficult to obtain well-defined bimetallic Pd-Rh structure. Indeed, Pd and Rh are immiscible at the thermal equilibrium bulk state over the whole composition range, therefore the alloy is in a segregated state at room temperature [12]. For this reason, alloys formed by these two metals have been obtained only in a metastable state by quenching the mixture at extremely high temperature, above 1000 K [13]. In the last decade, it was report that Pd-Rh alloyed system can be obtained at low temperature, mixing the two metal at the atomic level, using a polyols method where poly(N-vinyl-2-pyrrolidone) (PVP) acts as stabilizer and ethylene glycol as reducer [9,14]. Ham and co-workers used theoretical calculations to demonstrate that the addition of Rh to Pd enhance the activity of pure Pd in the formic acid dehydrogenation, enhancing the selectivity to H_2 and avoiding the formation of CO which acts as poison for Pd catalysts [15]. The beneficial effect obtained by introducing Rh to Pd was attributed to a contraction of the Pd-Pd distance and the increase in the electron density in surface Pd atoms compared to pure Pd [15]. Formic acid, that can be produced from lignocellulosic biomass, has attracted extensive attention as a promising renewable liquid-phase hydrogen donor due to properties such as high volumetric hydrogen content (4.4%), liquid state at room temperature, high stability, environmental benignity and non-toxicity [16,17]. Formic acid decomposition in the liquid phase has been studied using a range of heterogeneous catalysts [18]. Heterogeneous catalysts, based on supported metal nanoparticles, such as, Pd, Au and the corresponding bimetallic systems have been reported in both the past and recent years [19,20]. However, the preparation of an active, selective and above all stable catalyst still represents a challenge.

Our group has a good experience in the preparation of bimetallic systems (e.g. Au-Pd, Au-Pt, Au-Ru) using the immobilization of preformed metal nanoparticles with an alloy structure [21]. In this work, we utilized this technique to prepare Pd-Rh nanoparticles using polyvinyl alcohol (PVA) as protecting agent and $NaBH_4$ as

reducing agent. We choose highly graphitized carbon nanofibers (HHT) as support. Indeed, we have recently reported that the utilization of these materials can improve the catalytic activity of supported Pd nanoparticles compared to other carbonaceous supports [22]. The synthesized catalysts were tested in the decomposition of formic acid to produce hydrogen in liquid phase reaction conditions. The structure of the catalysts before and after reaction was carefully studied by means of electron microscopy. The most active catalysts were then tested in the liquid-phase hydrogenation of muconic acid in presence of formic acid as hydrogen donor. This is an important reaction to obtain bio-adipic acid starting from renewable resources and using the concept of *in situ* hydrogen generation using high content H donors like formic acid, at mild reaction conditions [23,24].

2 Experimental method

2.1 Materials and chemicals

Rhodium(II) acetate ($Rh(CO_2CH_3)_2]_2$) was purchased from Alfa Aesar (99.99 %) and sodium tetrachloropalladate (II) (Na_2PdCl_4, 99.99 %), sodium borohydride ($NaBH_4$, 99.99 %) and poly(vinyl alcohol) (PVA, average molar weight 10,000, 87-89 % hydrolyzed) were used without any pre-treatment for the catalysts synthesis and they were purchased from Sigma-Aldrich (Haverhill, MA, USA). All the catalytic tests were carried out using Formic acid (≥95%, Sigma-Aldrich) and deionised water and ethanol (≥95%, Sigma-Aldrich) as the substrate and the solvent, respectively. CNFs PR24-HHT (High Heat Treated carbon nanofiber) were obtained from Applied Science Company (Cedarville, OH, USA).

2.2 Catalysts preparation

In a typical sol immobilization procedure [25], the catalyst was prepared adding the solution of the metal precursor salts (Na_2PdCl_4, $[Rh(CO_2CH_3)_2]_2$; Table 1) and the capping agent PVA (M/PVA=1/0.5 (wt/wt)) in 0.5 L of H_2O/EtOH=1/1 vol/vol. Then, a fresh aqueous solution of $NaBH_4$ (M/$NaBH_4$=1/8 (mol/mol)) was added at once. The colloidal metal solution was supported on HHT CNFs (0.495g) under vigorous stirring. By using sulphuric acid, the suspension was acidified to pH 2 and stirred for 30 min in order to ensure the full immobilization of the nanoparticles on the support. The solid was filtered, washed with 0.5L of H_2O and dried in oven at 80°C for 1 day.

Table 1: Summary of the amount of the metals for the preparation of the sol.

Pd-Rh Ratio	*Pd (mmolx10^{-2})*	*Rh (mmolx10^{-2})*
Pd	4.70	-
Pd_8Rh_2	3.78	0.95
Pd_6Rh_4	2.86	1.90
Pd_4Rh_6	1.92	2.88
Pd_2Rh_8	0.97	3.86
Rh	-	4.86

2.3 Catalytic tests

Formic acid dehydrogenation: Liquid-phase Formic acid decomposition was carried out in a two-necked 100 mL round-bottom flask placed in a water bath equipped with a magnetic stirrer and a reflux condenser.

Typically, 10 mL of an aqueous solution 0.5M of HCOOH was placed in the reactor and the reaction temperature was set-up at 30°C. The Formic Acid/metal molar ratio is 2000:1 and once the solution reached the desired temperature, the solution was stirred at 1400 rpm. At these experimental conditions we have shown previously we operate under kinetic regime[22]. Recycle tests were performed on the most active catalysts using 25mL of an aqueous solution of HCOOH 0.5M in a 250 mL round-bottom flask at the same experimental conditions of the reaction previously discussed.

Muconic acid (MA) hydrogenation: 25.3 mg of MA were placed in a round bottom flask with 15 mL of distilled water. Then 32 mg were added in 10 ml flask to have a MA/FA ratio of 1/4 (mol/mol). Water was used as solvent for both the solutions. FA was therefore added to MA solution. The final concentration of MA was 0.007M. Finally, the catalyst was added with a MA/metal ratio of 200/1 (mol/mol). The reactions were performed at 30 °C with a stirring rate of 1400 rpm. The reactor was left open to facilitate FA decomposition toward the production of H_2. Periodic withdrawals were performed at different reaction times and the products were analysed by High Performance Liquid Chromatography (HPLC).

Product analysis: Formic acid and muconic acid conversion were analysed using high-performance liquid chromatography (HPLC). In particular an H+ chromatographic column was used (Alltech OA- 10,308, 300 mm_7.8 mm) with UV detector settled at 210 nm. Liquid samples were withdrawn periodically (200 µL) and diluted to 5 mL with H_3PO_4 solution (0.1 wt %) which was also the eluent of the analysis. The isocratic eluent flow was set at 0.4 ml min-1. The gas phase was analyzed by gas chromatography (Agilent, mod. 7890) equipped with a TCD detector and a proper set up for the quantification of H_2 and CO.

2.5 Catalyst characterization

Transmission electron microscopy experiments were performed on a double Cs aberration-corrected FEI Titan^3 Themis 60–300 microscope equipped with a monochromator, a X-FEG gun and a high efficiency XEDS

ChemiSTEM, which consists of a 4-windowless SDD detectors. HR-STEM imaging was performed at 200 kV and using a high-angle annular dark-field (HAADF) detector with a camera length of 11.5 cm. The HAADF-STEM technique is sensitive to the atomic number of the elements, whose intensity is roughly proportional to the square of the atomic number (Z^2), and it makes possible to distinguish small nanoparticles supported on light supports. XEDS mappings were performed using a beam current of 200 pA and a dwell time per pixel of 128 µs. To improve the visual quality of the elemental maps obtained, these were filtered using a Gaussian blur of 0.8 using Velox software. Based on the STEM-HAADF images of the catalysts, the diameters of more than 200 metal particles randomly selected were measured and the corresponding metal particle size distributions (PSD) were determined. Based on these PSDs, the average particle diameter (d) was calculated according to the following expression: $d = \sum n_i d_i / \sum n_i$, where $n_i \geq 200$. Likewise, the total metal dispersion was calculated according to $D = N_s/N_t$, where N_s is total number of surface metal atoms and N_t is total number of atoms in the metal particle. For particle size calculation ImageJ software was used.

Metal loading and metal leaching were analyzed by Inductively coupled plasma optical emission spectroscopy (ICP-OES) using a Perking Elmer Optima 8000 emission.

Results

Pd_xRh_y/HHT bimetallic catalysts with different Pd:Rh atomic ratio, and the corresponding Pd and Rh monometallic ones were prepared by sol immobilization method using polyvinyl alcohol (PVA) as protective agent (Table 2). Compared to the classical preparation method [22] where pure water is used a solvent, a mixture of ethanol and water was used due to the low solubility of $[Rh(CO_2CH_3)_2]_2$ in water.

TEM-STEM results

The catalysts were characterized at the sub-nanometric scale by transmission electron microscopy. TEM image of the monometallic Pd/HHT was reported elsewhere [22] and a STEM image of Rh/HHT is reported in figure S1 in the supporting information. Both monometallic catalysts showed a similar average particle size of 3.2 and 3.5 nm, respectively (Table 2) with particles well dispersed on the surface of the carbon nanofibers. Figures 1-4 show representative results obtained by STEM and investigation of the Pd-Rh bimetallic systems. The catalysts show a similar average particle size in the range of 2.5-3.2 nm, table 2, with a narrow particle size distribution, as shown in Figures 1c-4c. STEM-XEDS analysis was performed on individual particles to analyse their composition (Figures 1-4, Table 2). Line profiles of single particles are also included to illustrate the formation of bimetallic nanoparticles. Regarding sample with noPd_2Rh_8, (Figure 1) an average particle size of 2.6 nm was obtained, although some big agglomeration of tiny crystallites was found in the sample (Figure S2). Interestingly, the particles included in these agglomerations have a low content of Rh (< 10%) or even they are pure Pd (Figure S2b). The small particles are always made of both Rh and Pd, with a Pd-Rh ratio different from particle to particle and average Pd-Rh molar ratio of 40:60 (Table 2, Figure 1b).

Pd_4Rh_6 consists of particles with an average particle size of 3.2 nm (Table 2), with a broader particle distribution, (Figure 2). All the particles analysed were bimetallic with an average molar ratio of 49:51 (Pd:Rh), which indicates an enrichment of Pd, if we compare with the nominal composition (40:60). This composition also varies from particle to particle, (Figure 2b). In addition, in this case, large aggregates were observed (Figure S3a) with a lower content of Rh (Pd-Rh ratio of 79:21) in comparison with the one obtained for the small particles, (Figure S3b).

Particles with an average size of 2.5 were found for Pd_6Rh_4 catalyst (Table 2), with the presence of large aggregations of particles, (Figure S4). STEM-XEDS analysis (Figure 3) confirms the presence of Pd-Rh bimetallic particles with an average molar ratio of 69:31, which again show a higher Pd content that what it was expected. Moreover, for this sample the Pd-Rh relative content varies from particle to particle, (Figure 3b).

Pd_8Rh_2 shows highly and homogeneously dispersed metal nanoparticles with an average size of 2.9 nm and no aggregates were observed, (Figure 4). Particles exhibit an enrichment of Pd, with an average Pd:Rh atomic ratio of 90:10, which it is also higher than the nominal one of 80:20.

STEM-XEDS analysis performed on individual particles demonstrated that almost all the particles were Pd-Rh bimetallic, although the content of Rh is lower than the nominal one in all the prepared catalysts. Additionally, monometallic Rh and Pd particles were not observed. In order to demonstrate the formation of the bimetallic nanoparticles, EDS line profiles of isolated nanoparticles are included in figures 1-4. In all the analysed nanoparticles, we can observe the signals of Rh and Pd inside of the individual particles. Although the presence of really small particle size of 2-6 nm complicated the analysis the obtained line profiles may indicate a relatively homogenous distribution of both metal and that there is not any preferential distribution of the elements such core-shell structure. To understand the discrepancy between nominal and calculated Pd:Rh atomic ratio, we utilized the inductively coupled plasma optical emission spectroscopy (ICP-OES) to analyse the metal loading of the synthesised catalysts, (Table 2). The analysis performed on the filtrated solution, after the immobilization of the metal colloid on the carbon nanofibers, revealed the presence of Rh in solution. The same problem has been detected for the monometallic Rh catalyst which shows a calculated leading of 0.91% instead of the nominal one of 1%.

Table 2 Nominal and calculated Pd-Rh molar ratio and average particle size for the Pd_x-Rh_y catalysts.

Catalyst	*Nominal Pd-Rh Molar Ratio*	*Calculated Pd-Rh Molar Ratio (EDX-TEM)*	*Calculated Pd-Rh Molar Ratio (ICP)*	*Average particle size (nm)*
Pd	-	-	-	3.2 ± 0.8
Pd used	-	-	-	4.5±1.3
Pd_8Rh_2	80:20	90:10	87-13	2.9±0.9
Pd_8Rh_2 used	80:20	95:5	93-7	4.5±1.0
Pd_6Rh_4	60:40	69:31	73-27	2.5±0.6
Pd_6Rh_4 used	60:40	81:19	84-16	3.0±0.7
Pd_4Rh_6	40:60	49:51	47-53	3.4±1.3
Pd_2Rh_8	20:80	40:60	38-62	2.6±0.7
Rh	-	-	-	3.5±1.1

Figure 1 A) STEM-HAADF image of Pd_2Rh_8 catalyst, B) particle size distribution, C-F) STEM-XEDS of single nanoparticles (Pd-Rh atomic ratio: 1) 75:25, 2) 71:29 3) 20:80 4) 63:27 5) 52:48 6) 60:40 7) 62:38 8) 81:19 9) 29:71) and G-H) Line profile of the particle 1 and 5 respectively.

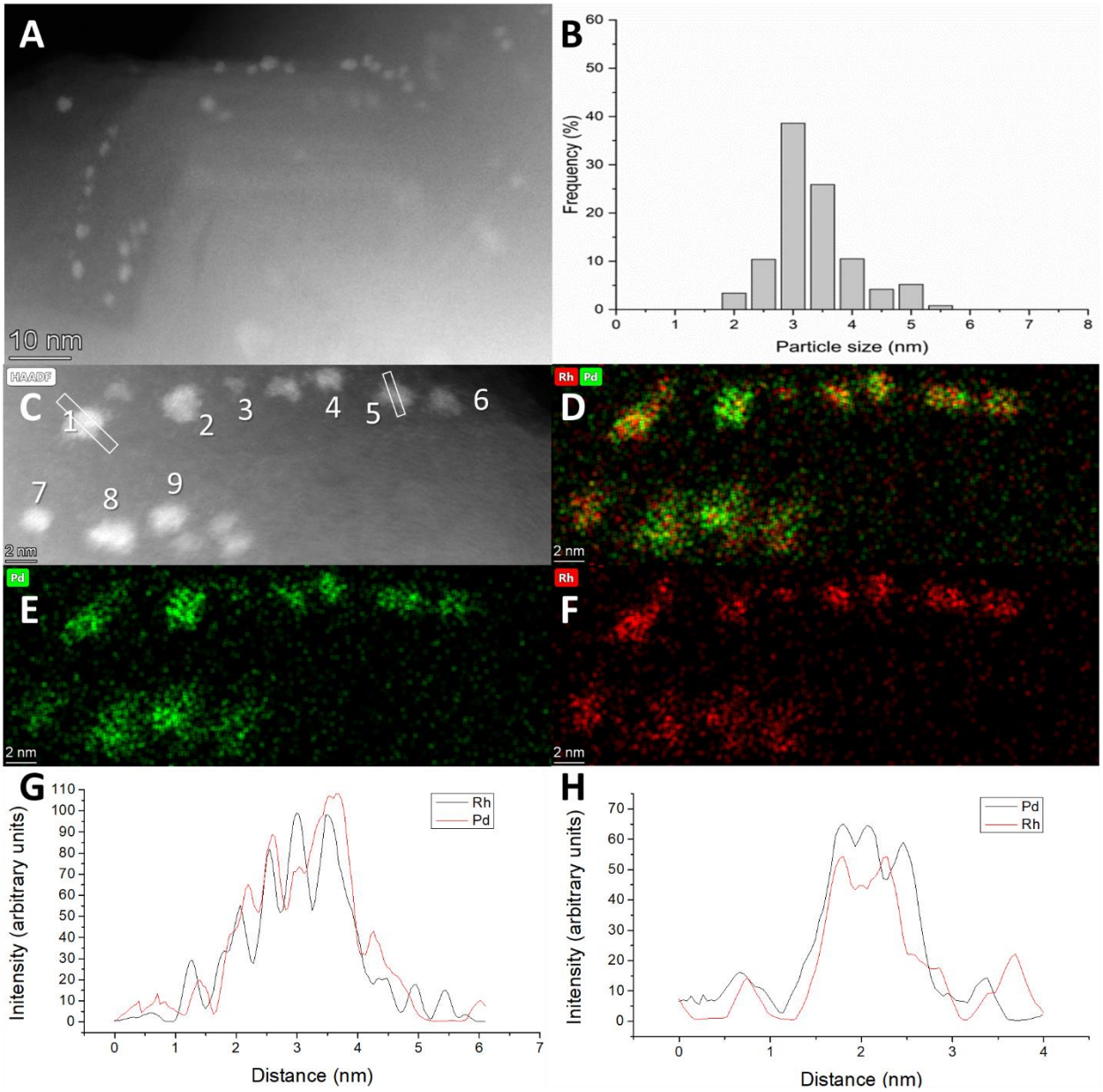

Figure 2 A) STEM-HAADF image of Pd_4Rh_6 catalyst, B) particle size distribution, C-F) STEM-XEDS of single nanoparticles (Pd-Rh atomic ratio: 1) 67:33, 2) 40:60, 3) 28:72, 4) 15:85, 5) 60:40, 6) 75:25, 7) 57:43, 8) 59:41, 9) 53:47) and G-H) Line profile of the particle 1 and 9 respectively.

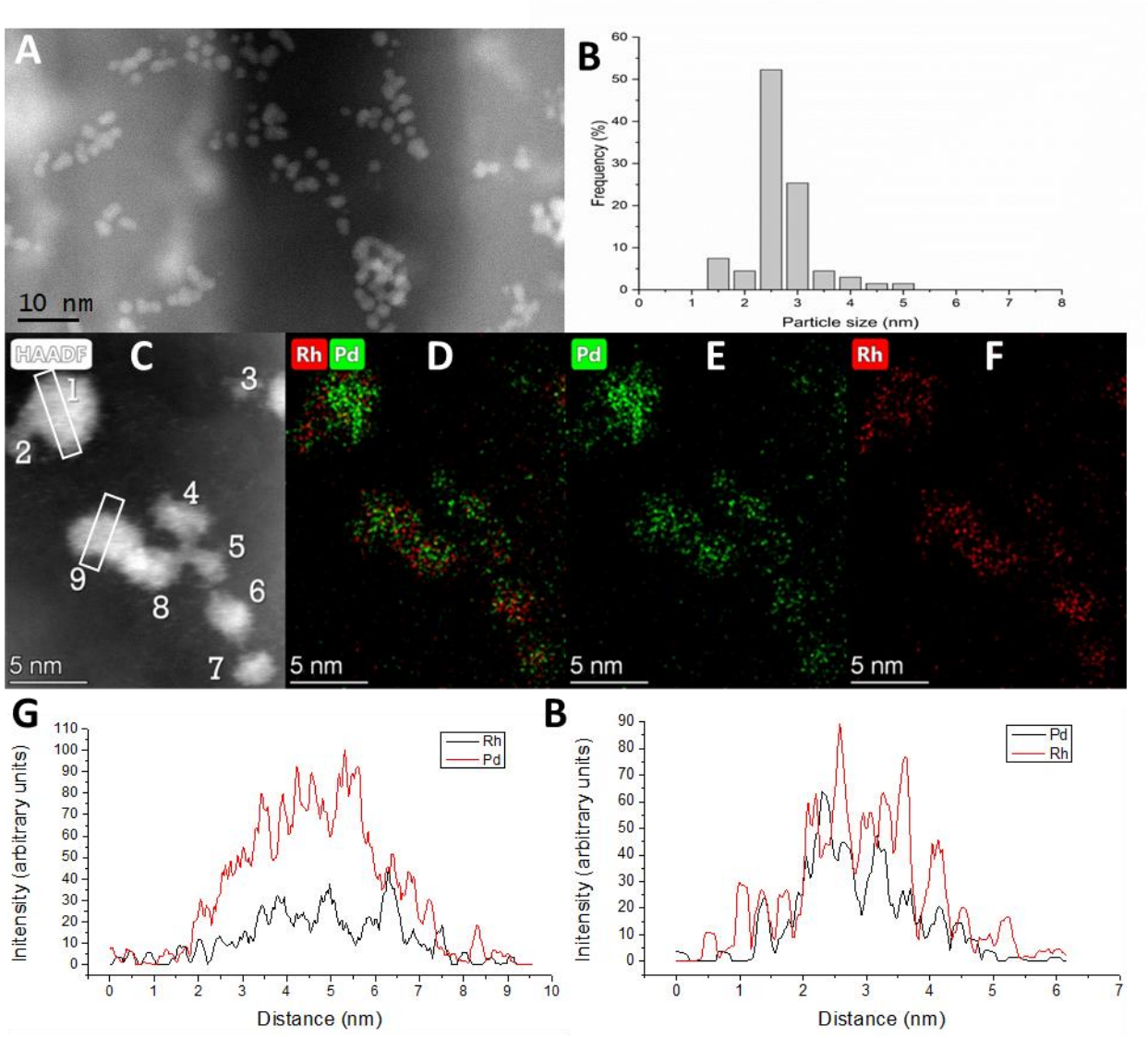

Figure 3 A) STEM-HAADF image of Pd_6Rh_4 catalyst, B) particle size distribution, C-F) STEM-XEDS of single nanoparticles (Pd-Rh atomic ratio: 1) 40:60, 2) 62:38, 3) 89:11, 4) 75:25, 5) 67:33, 6) 62:38) and G-H) Line profile of the particle 2 and 3 respectively.

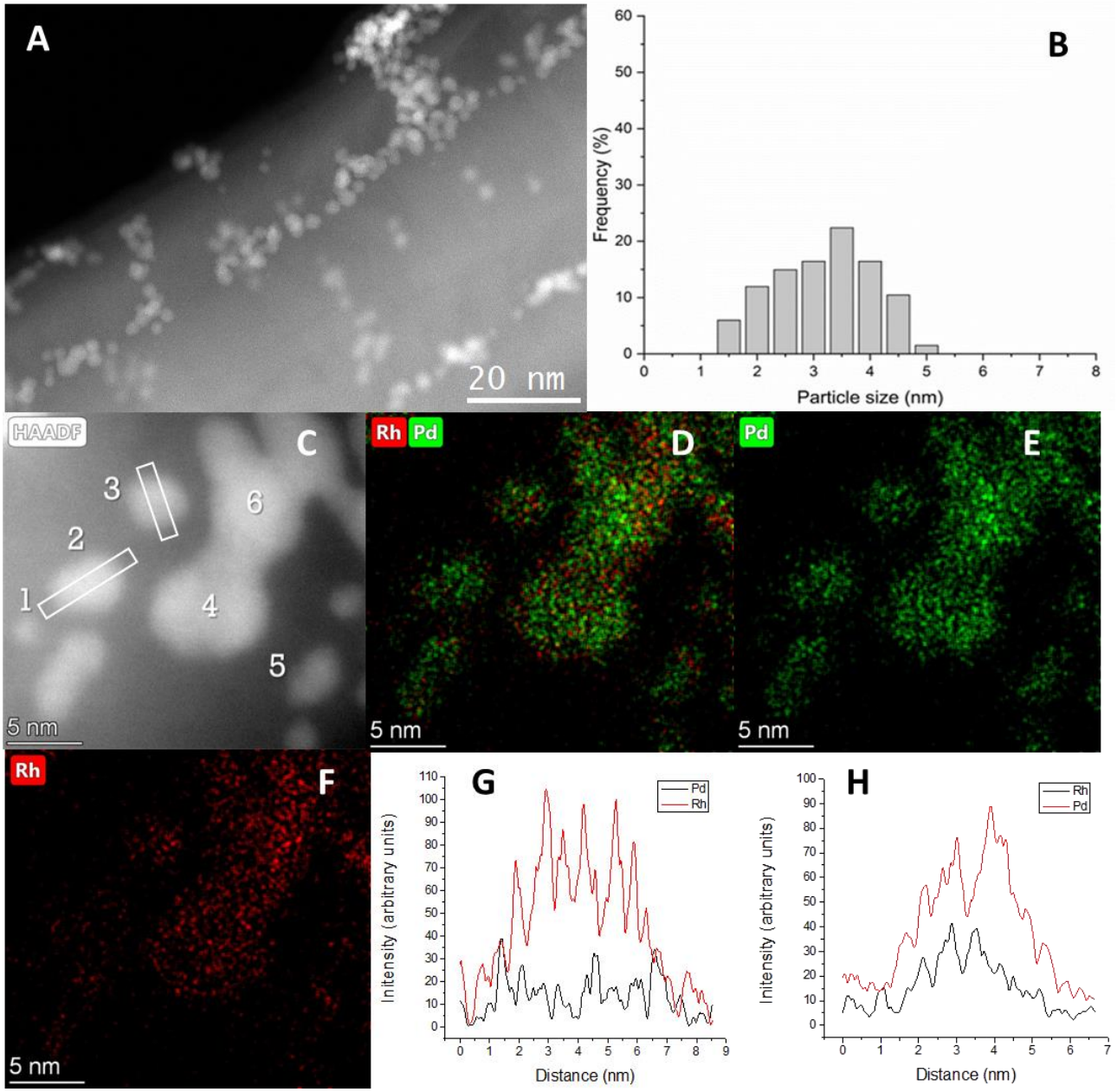

Figure 4 A) STEM-HAADF image of Pd_8Rh_2 catalyst, B) particle size distribution, C-F) STEM-XEDS of single nanoparticles (Pd-Rh atomic ratio: 1) 92:8, 2) 82:18, 3) 99:1, 4) 90:10, 5) 89:11) and G-H) Line profile of the particle 4 and 6 respectively.

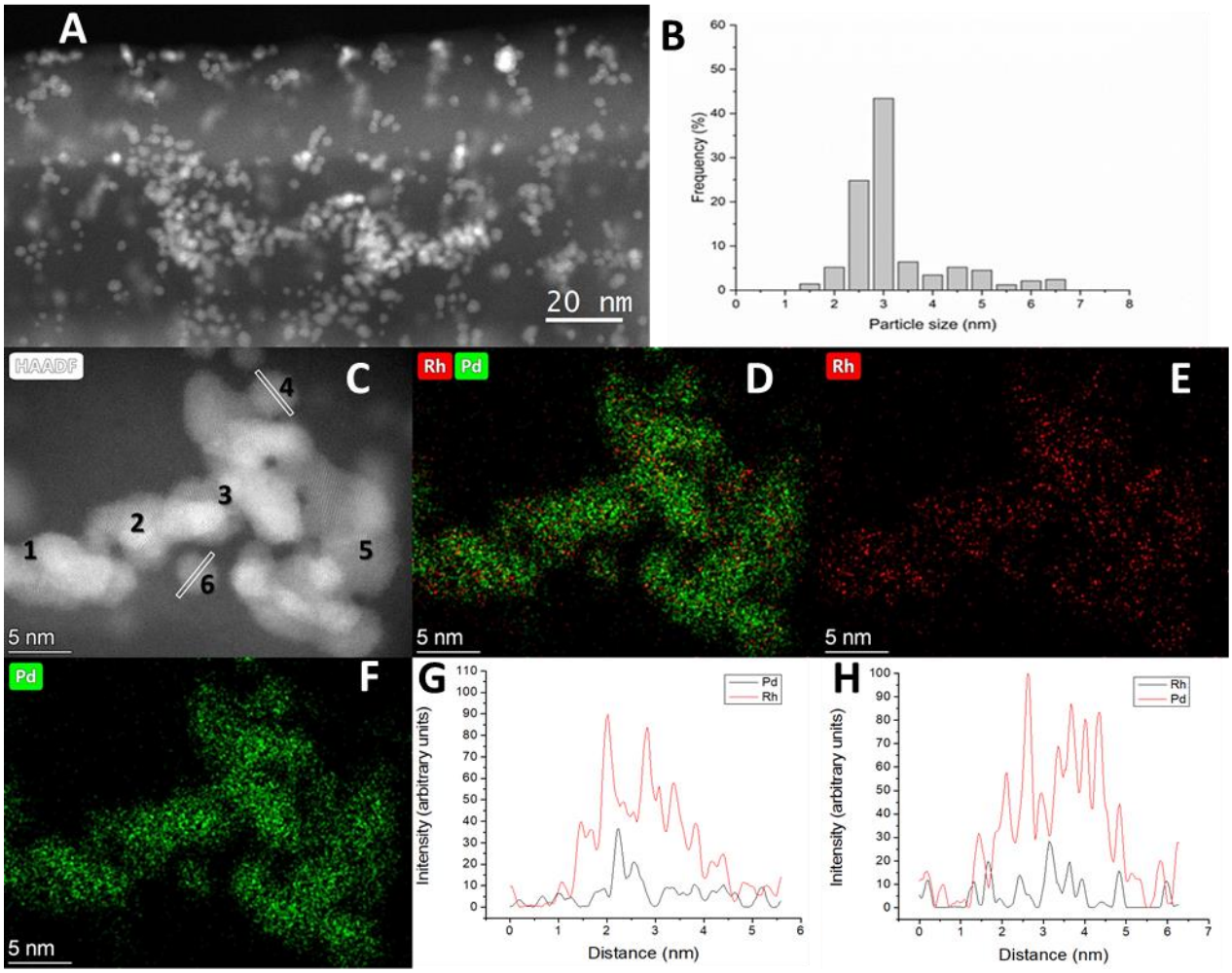

3 Catalytic activity

The catalytic performance of the Pd-Rh catalysts was evaluated in the liquid-phase decomposition of formic acid as a model reaction for hydrogen generation (Reaction conditions, 0.5 M HCOOH in water, 30 °C, stirring rate of 1400 rpm, substrate/metal molar ratio of 2000). The decomposition of formic acid follows two main pathways, (i) dehydrogenation ($HCOOH \rightarrow CO_2 + H_2$, ΔG=-48.4 $kJmol^{-1}$) and (ii) dehydration ($HCOOH \rightarrow CO + H_2O$, ΔG=-28.5 $kJmol^{-1}$). The reaction conditions, in particular stirring rate and substrate/metal molar ratio were optimised in previous reports, in order that the reaction is taking place in chemical kinetic regime [22]. Figure 5 presents the catalytic activity of the catalysts prepared by varying the Pd-Rh atomic ratio. To better correlate the effect of the metal ratio and the activity, the calculated Pd-Rh instead of the nominal molar ratio will be now considered. The activity is expressed as mol of formic acid reacted per total mol of metal per hour and calculated after 5 minutes of reaction. The highest initial activity was obtained using $Pd_{90}Rh_{10}$ (1793 h^{-1}), followed by monometallic Pd and $Pd_{69}Rh_{31}$ which showed similar results (979 and 921 h^{-1}, respectively). Increasing the Rh content, the activity progressively decreased and the monometallic Rh showed very low

activity, (Figure 5). However, this trend was not followed by $Pd_{40}Rh_{60}$ which showed an activity two times higher (696 h^{-1}) than $Pd_{48}Rh_{52}$ (341 h^{-1}). We could not find the reason to fully justify the observed catalytic trend. Indeed, the two catalysts showed similar bimetallic structure, even the particle size is slightly larger for $Pd_{48}Rh_{52}$ (3.4 nm) than the other bimetallic catalysts (2.4- 2.9 nm) (Table 2). In general, the influence of particle size in catalyst activity for this series of catalysts seem to be negligible compared to that of Pd-Rh composition. Table 3 presents a comparison of the activity of various Pd based bimetallic catalysts for the liquid phase dehydrogenation of formic acid under mild conditions. $Pd_{90}Rh_{10}$ shows an activity better of most of the catalysts presented in the literature. Figure 6 showed similar reaction profiles for all the catalysts and no evident deactivation phenomena seem to be present. $Pd_{90}Rh_{10}$ showed the highest conversion after 2h of reaction (81%). Interestingly $Pd_{69}Rh_{31}$, despite showing a similar initial activity than monometallic Pd, showed a higher conversion after 2h than this latter one (54 and 28%, respectively, Figure 6). The products detected in the gas phase were mainly CO_2 and H_2 with presence of CO under the detection limit of the instrument (5 ppm) for the bimetallic systems and of 12 ppm for the monometallic Pd catalyst. Therefore, these catalysts can be used for the production of H_2 in fuel cells, since CO is the main issue for chemical poisoning in the case of using hydrogen fuel cells for the generation of energy and it is important to be kept below 10 ppm level. Stability tests have been performed using $Pd_{90}Rh_{10}$, $Pd_{69}Rh_{31,}$ with the catalysts presenting the highest conversion after 2 h and compared to the Pd monometallic one, (Figure 7). Recycling experiments were carried out by filtering and using the catalyst in the next run without any further purification. Palladium catalyst rapidly deactivated after the first run, in agreement with previous studies, [22] (Figure 7a). Agglomeration and coalescence of the particles was observed, and the average particle size increased from 3.0 to 4.7 nm (Table 2). ICP analysis performed on the filtrated solution revealed the leaching of 5% of Pd during the reaction. Moreover, Pd active sites can be poisoned by the CO produced (11-15 ppm, in the different cycles). It is well known, indeed, that CO can poison Pd catalysts even when present at ppm level [26]. A similar trend was observed for $Pd_{90}Rh_{10}$, the most active catalyst. STEM analysis evidenced the coalescence of the particles with growing of the average particle size from 2.9 to 4.5 nm (Figure 8c). The STEM-XEDS analysis showed an enrichment in Pd of the particles, which have an average composition of 95:5 with the presence of segregated monometallic Pd particles (Table 2). ICP results demonstrated that this is due to the partial leaching of Rh in the reaction solution, whereas no leaching of Pd was observed. On the contrary, $Pd_{69}Rh_{31}$ showed a good stability during the 6 cycles, (Figure 7c). STEM analysis of the used catalyst evidenced a limited growing of the average particle size from 2.5 to 3.0 nm, (Table 2). The analysis of the atomic composition of the single nanoparticles showed an enrichment in Pd with a Pd-Rh atomic ratio of 81:19, (Figure 9b), due to the leaching of Rh in the solution. The high stability might be attributed to a catalyst with a Pd-Rh composition similar to the most active ones. The higher activity of the new phase is offset by the leaching of metal in the solution, and the conversion was constant during the 6 cycles. The partial Rh leaching observed for the bimetallic catalysts can be due to the fact that Pd-Rh structures are not stable upon hydrogen absorption/desorption, leading to a partial segregation of the two metals [13,27]. Probably, segregated Rh is more prone to leaching than when alloyed.

Figure 5 Activity vs Pd-Rh ratio in the formic acid dehydrogenation.

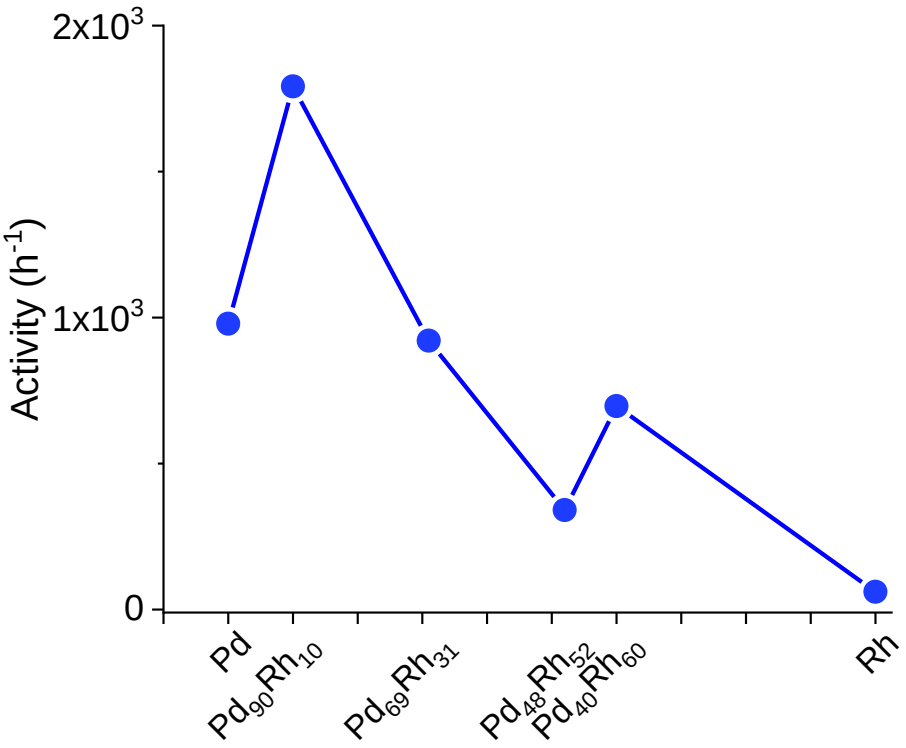

Figure 6 Reaction profiles for Pd-Rh catalysts in the formic acid dehydrogenation.

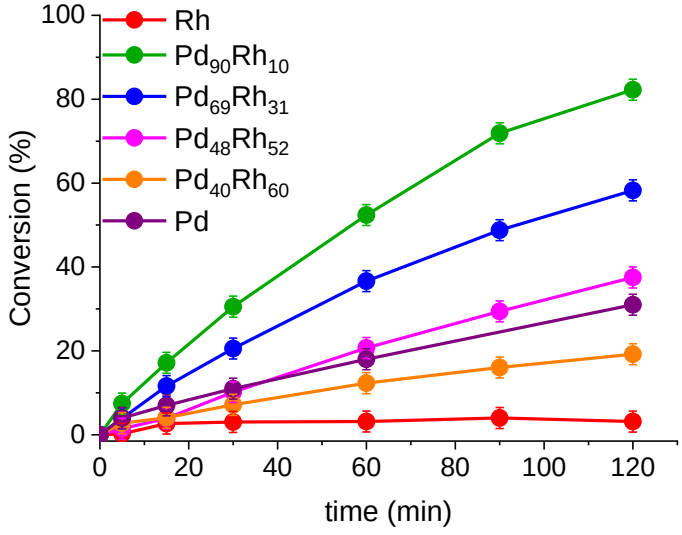

Table 3 Comparison of catalytic activity of Pd-based bimetallic catalysts for the liquid phase dehydrogenation of formic acid under mild conditions.

Catalyst	T (°C)	Reagent	TOF (h^{-1})		Ref.
			Initial	2 h	
$Pd_{90}Rh_{10}$/HHT	30	Formic acid (0.5 M)	1793		This work
$Pd_{69}Rh_{31}$/HHT	30	Formic acid (0.5 M)	921		This work
Pd/HHT	30	Formic acid (0.5 M)	979		This work
Pd/C	21	Formic acid (1.33 M)	18	15	[28]
	30		48	28	
$Au_{41}Pd_{59}$/C	50	Formic acid (1 M)	230		[29]
Ag@Pd (1:1)	35	Formic acid		156	[30]
Ag/Pd alloy (1:1)	20			144	[30]
$Ag_{42}Pd_{58}$	50	Formic acid (1 M)	382		[31]
Pd-MnO_x/SiO_2-NH_2	20	Formic acid (0.265 M)	140		[32]
	50		1300		
$Ag_{0.1}Pd_{0.9}$/rGO	25	Formic acid	105		[33]
PdNiAg/C	50	Formic acid (0.175 M)	85		[34]
$Pd_{50}Cu_{50}$/resin	75	HCOOH/HCOONa=9:1	810		[35]
20 wt% PdAu/C–CeO2	102	9.94 M formic acid–3.33 M sodium formate solution	832		[36]

Figure 7 Recycling tests for a) monometallic Pd, b) $Pd_{90}Rh_{10}$ and c) $Pd_{69}Rh_{31}$.

a)

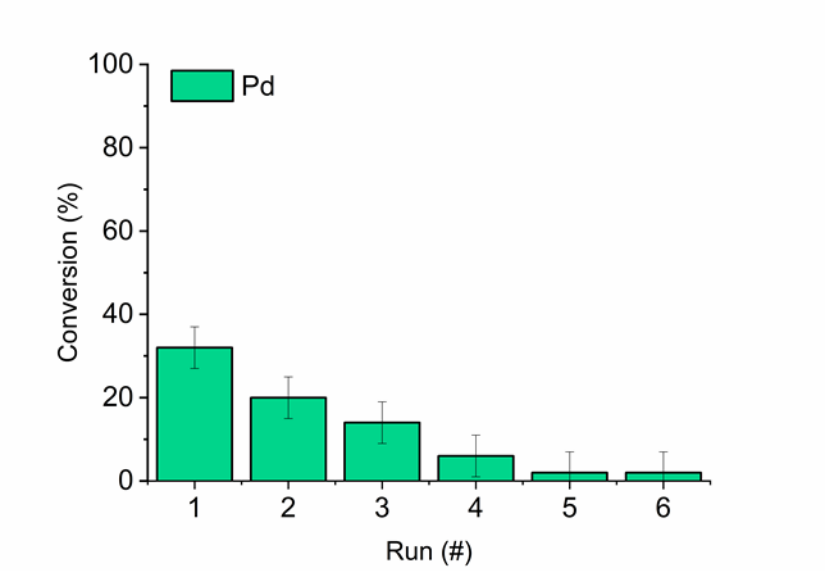

b)

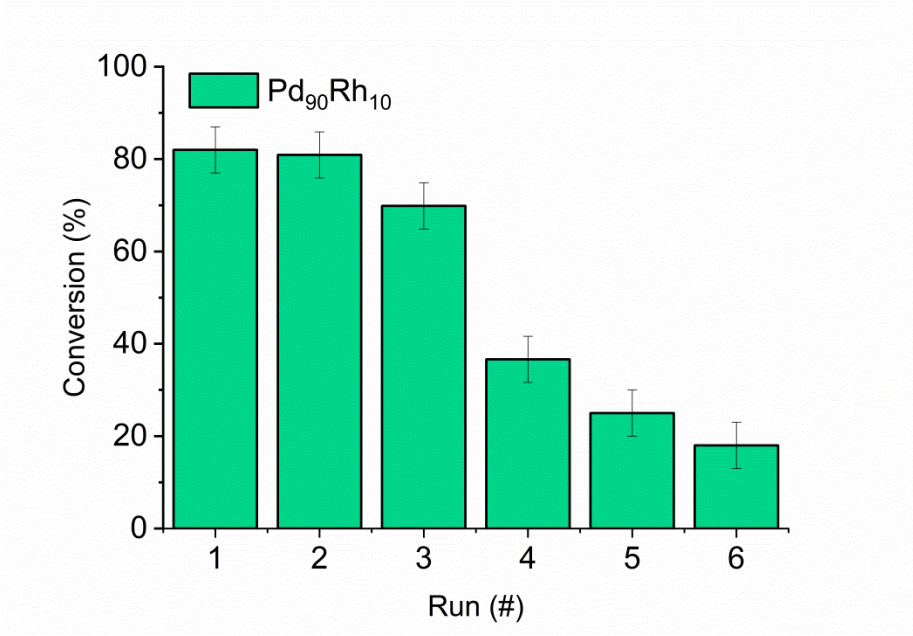

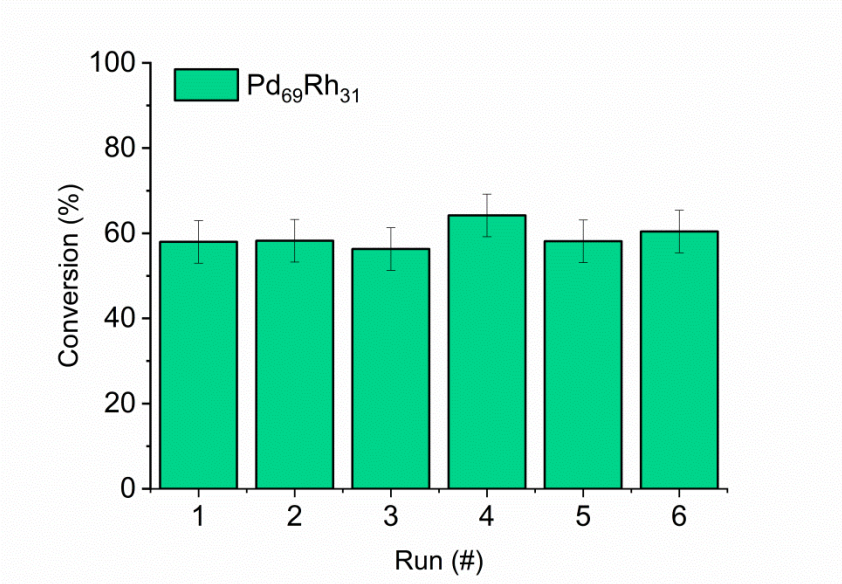

c)

Figure 8 a) STEM-HAADF image, STEM-XEDS of single nanoparticles and c) particle size distribution of $Pd_{90}Rh_{10}$ used catalyst.

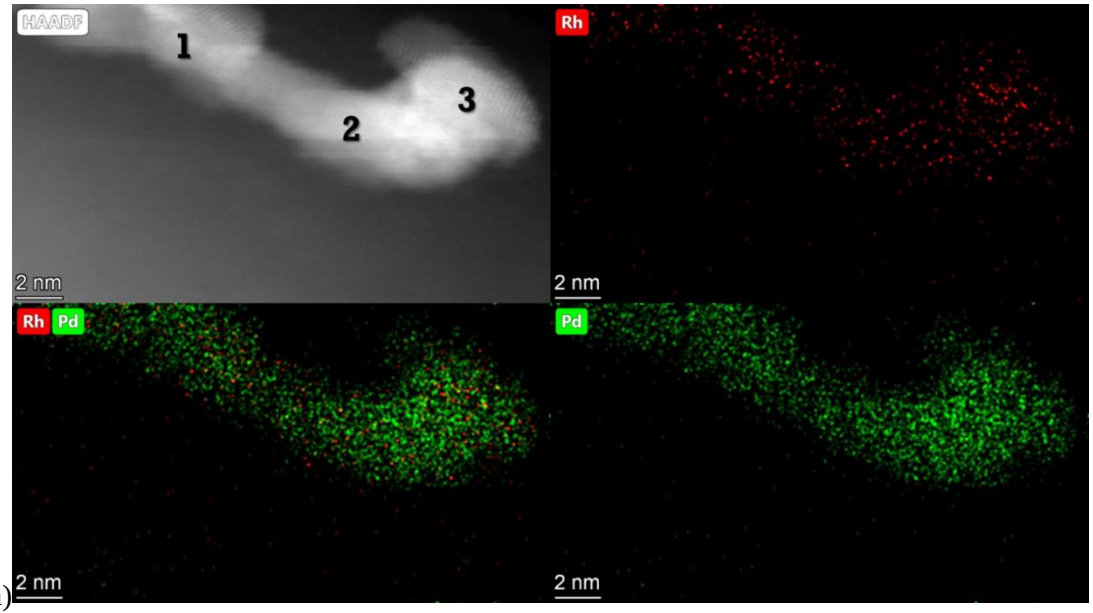

a)

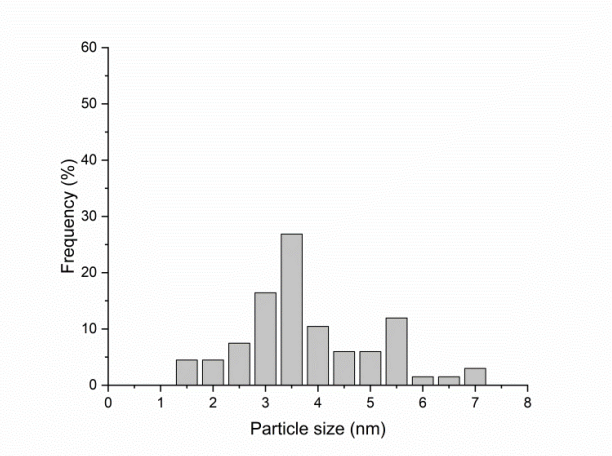

b)

Figure 9 a) STEM-HAADF image, STEM-XEDS of single nanoparticles and c) particle size distribution of $Pd_{69}Rh_{31}$ used catalyst.

a)

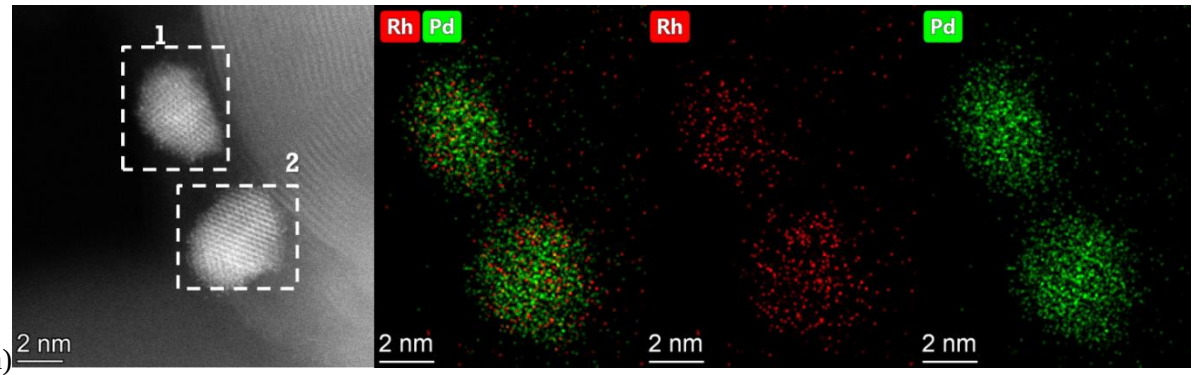

b)

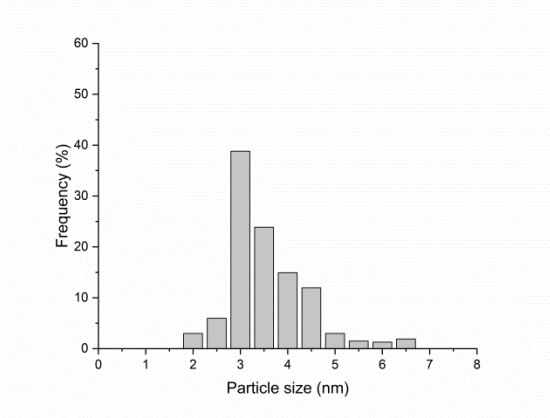

Many studies have reported the last 10 years, the utilization of formic acid as hydrogen source for the hydrogenation of biomass derived molecules [16]. In this work we utilized formic acid for the upgrade of muconic acid (MA), a molecule which can be obtained from cellulose and lignin to produce bio-adipic acid, (Scheme 1). The reaction proceeds in two-steps as we have recently shown [23]. In the first one, monounsaturated acids are produced ((2E)-hexenedioic acid and (3E)-hexenedioic acid), followed by the hydrogenation of the second C=C bond to obtain adipic acid.

Scheme 1 Conversion of muconic acid into bioadipic acid.

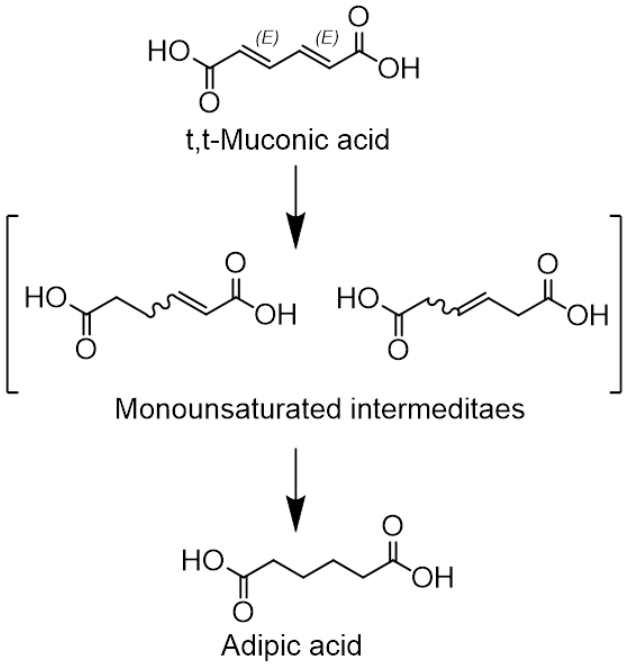

Pt and Pd based catalysts have been used for this reaction [23,37], using molecular hydrogen. However, Pd based ones showed the best activity even under mild conditions. Therefore, we combine the ability of Pd catalyst to generate hydrogen from formic acid (H-source) and at the same time to activate H_2 under mild conditions to hydrogenate muconic acid to bio-adipic acid. Muconic acid hydrogenation was performed under similar reaction conditions utilized for the dehydrogenation of formic acid (Reaction conditions, 0.007 M MA in water, MA/Formic acid ratio of 1/4 (mol/mol), 30 °C, stirring rate of 1400 rpm, substrate/metal molar ratio of 200). The two most active bimetallic catalysts, $Pd_{90}Rh_{10}$ and $Pd_{69}Rh_{31}$ were compared to monometallic Pd. In figure 10 it is plotted the concentration of the reactant MA, the mono unsaturated intermediates and adipic acid as a function of reaction time. All the catalysts were highly active in the first step, almost quantitatively converting MA to the intermediates after 1h of reaction. However only the two bimetallic catalysts were able to convert the intermediates to adipic acid, in particular in the case of $Pd_{69}Rh_{31}$. The lower activity of Pd can be attributed to the lower activity and stability in the generation of hydrogen from formic acid compared to bimetallic counterparts. However, it can be observed that after 2h of reaction the concentration of the products remains stable. Future studies will be performed to improve the catalytic performance of the present catalysts and to understand the reason of deactivation in the muconic acid hydrogenation in presence of formic acid as hydrogen donor.

Figure 10 Activity of a) monometallic Pd, b) $Pd_{90}Rh_{10}$ and c) $Pd_{69}Rh_{31}$ catalysts in the muconic acid hydrogenation using formic acid as hydrogen donor.

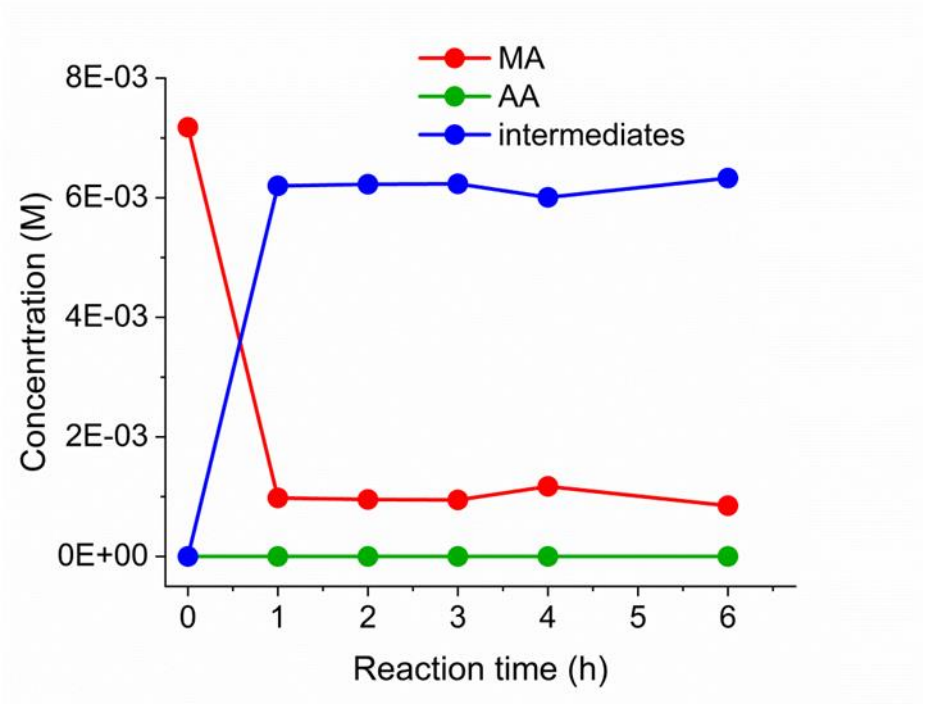

a)

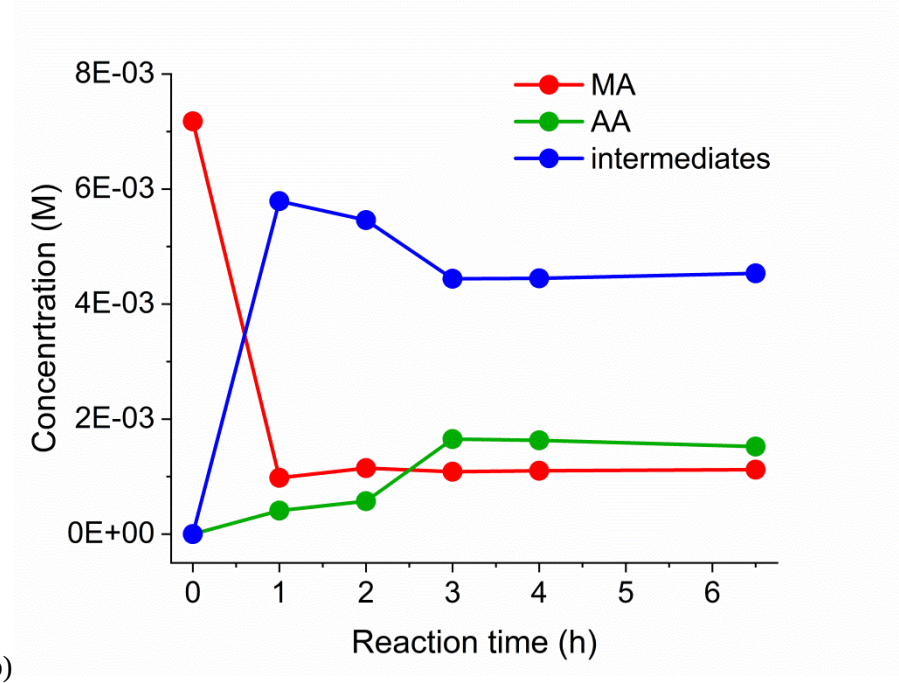

b)

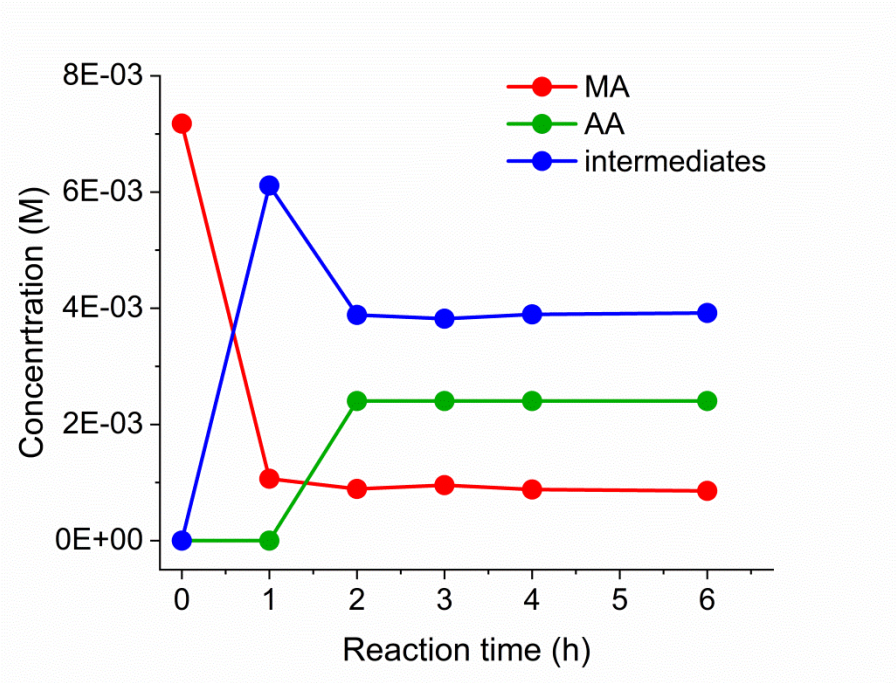

c)

Conclusions

A series of preformed colloidal Pd_xRh_y nanoparticles and the corresponding monometallic supported Pd and Rh nanoparticles were prepared by sol immobilization method and deposited on highly graphitized carbon nanofibers (HHT). Using this technique we report for the first time, the ability to prepare preformed bimetallic random alloyed Pd-Rh nanoparticles with average particle size in the range of 2-4 nm even at low temperature as confirmed by STEM-HAADF and STEM-XEDS analyses. However, the composition of the particles is not homogeneous from particle to particle and a general enrichment in Pd was observed compared to the nominal Pd-Rh ratio. These results were attributed to the unsuccessful quantitative immobilization of Rh, as evidenced by ICP analysis. Bimetallic catalysts showed good activity in the dehydrogenation of formic acid in liquid phase, in particular for Pd-rich bimetallic systems ($Pd_{90}Rh_{10}$ and $Pd_{69}Rh_{31}$). Comparing the product analysis of liquid and gas phase products, we concluded that the major reaction pathway towards the production of CO_2 and H_2 was obtained for all the catalysts, with minor formation of CO in the range of 5-15 ppm. However, in the case of monometallic Pd, traces of CO (11-15 ppm) was observed. A good stability during 6 consecutive runs was observed for $Pd_{69}Rh_{31}$ compared to monometallic Pd which rapidly deactivate. The low stability of this latter one was attributed to the growing of particle size due to coalescence of the particle, partial Pd leaching and presence of CO which acts as poison for Pd-based catalysts. Furthermore, monometallic Pd, $Pd_{90}Rh_{10}$ and $Pd_{69}Rh_{31}$ were tested in the muconic acid hydrogenation using formic acid as hydrogen donor, under mild conditions. The catalysts showed good activity for the first step of the reaction, towards the production of monounsaturated products. Only in the case of using bimetallic catalysts the second step of the reaction towards the formation of adipic acid was enhanced.

References

[1] M. Besson, P. Gallezot, C. Pinel, Conversion of biomass into chemicals over metal catalysts, Chem. Rev. 114 (2014) 1827–1870. https://doi.org/10.1021/cr4002269.

[2] T. Mallat, A. Baiker, Oxidation of alcohols with molecular oxygen on solid catalysts, Chem. Rev. 104 (2004) 3037–3058. https://doi.org/10.1021/cr0200116.

[3] I. Favier, D. Pla, M. Gómez, Palladium Nanoparticles in Polyols: Synthesis, Catalytic Couplings, and Hydrogenations, Chem. Rev. 120 (2020) 1146–1183. https://doi.org/10.1021/acs.chemrev.9b00204.

[4] C.E. Chan-Thaw, A. Savara, A. Villa, Selective benzyl alcohol oxidation over pd catalysts, Catalysts. 8 (2018). https://doi.org/10.3390/catal8100431.

[5] W. Wu, H. Jiang, Palladium-Catalyzed Oxidation of Unsaturated Hydrocarbons Using Molecular Oxygen, Acc. Chem. Res. 45 (2012) 1736–1748. https://doi.org/10.1021/ar3000508.

[6] F. Liao, T.W.B. Lo, S.C.E. Tsang, Recent Developments in Palladium-Based Bimetallic Catalysts, ChemCatChem. 7 (2015) 1998–2014. https://doi.org/10.1002/cctc.201500245.

[7] L. Zhang, Z. Xie, J. Gong, Shape-controlled synthesis of Au-Pd bimetallic nanocrystals for catalytic applications, Chem. Soc. Rev. 45 (2016) 3916–3934. https://doi.org/10.1039/c5cs00958h.

[8] D.A. Colby, R.G. Bergman, J.A. Ellman, Rhodium-catalyzed C-C bond formation via Heteroatom-directed C-H bond activation, Chem. Rev. 110 (2010) 624–655. https://doi.org/10.1021/cr900005n.

[9] G.W. Piburn, H. Li, P. Kunal, G. Henkelman, S.M. Humphrey, Rapid Synthesis of Rhodium-Palladium Alloy Nanocatalysts, ChemCatChem. 10 (2018) 329–333. https://doi.org/10.1002/cctc.201701133.

[10] W. Ye, S. Kou, X. Guo, F. Xie, H. Sun, H. Lu, J. Yang, Controlled synthesis of bimetallic Pd-Rh nanoframes and nanoboxes with high catalytic performances, Nanoscale. 7 (2015) 9558–9562. https://doi.org/10.1039/c4nr06917j.

[11] L. Soler, A. Casanovas, J. Ryan, I. Angurell, C. Escudero, V. Pérez-Dieste, J. Llorca, Dynamic Reorganization of Bimetallic Nanoparticles under Reaction Depending on the Support Nanoshape: The Case of RhPd over Ceria Nanocubes and Nanorods under Ethanol Steam Reforming, ACS Catal. 9 (2019) 3641–3647. https://doi.org/10.1021/acscatal.9b00463.

[12] S.N. Tripathi, S.R. Bharadwqj, The Pd-Rh (Palladium-Rhodium) system, J. Phase Equilibria. 15 (1994) 208–212. https://doi.org/10.1007/BF02646369.

[13] H. Noh, J.D. Clewley, T.B. Flanagan, A.P. Craft, Hydrogen-induced phase separation in Pd-Rh

alloys, J. Alloys Compd. 240 (1996) 235–248. https://doi.org/10.1016/0925-8388(95)02193-0.

[14] H. Kobayashi, H. Morita, M. Yamauchi, R. Ikeda, H. Kitagawa, Y. Kubota, K. Kato, M. Takata, S. Toh, S. Matsumura, Nanosize-Induced Drastic Drop in Equilibrium Hydrogen Pressure for Hydride Formation and Structural Stabilization in Pd–Rh Solid-Solution Alloys, J. Am. Chem. Soc. 134 (2012) 12390–12393. https://doi.org/10.1021/ja305031y.

[15] J. Cho, S. Lee, S.P. Yoon, J. Han, S.W. Nam, K.-Y. Lee, H.C. Ham, Role of Heteronuclear Interactions in Selective H_2 Formation from HCOOH Decomposition on Bimetallic Pd/M (M = Late Transition FCC Metal) Catalysts, ACS Catal. 7 (2017) 2553–2562. https://doi.org/10.1021/acscatal.6b02825.

[16] J. Eppinger, K.-W. Huang, Formic Acid as a Hydrogen Energy Carrier, ACS Energy Lett. 2 (2017) 188–195. https://doi.org/10.1021/acsenergylett.6b00574.

[17] N. Onishi, M. Iguchi, X. Yang, R. Kanega, H. Kawanami, Q. Xu, Y. Himeda, Hydrogen Storage Technology: Development of Effective Catalysts for Hydrogen Storage Technology Using Formic Acid (Adv. Energy Mater. 23/2019), Adv. Energy Mater. 9 (2019) 1970090. https://doi.org/10.1002/aenm.201970090.

[18] Z. Li, Q. Xu, Metal-Nanoparticle-Catalyzed Hydrogen Generation from Formic Acid, Acc. Chem. Res. 50 (2017) 1449–1458. https://doi.org/10.1021/acs.accounts.7b00132.

[19] H. Dai, B. Xia, L. Wen, C. Du, J. Su, W. Luo, G. Cheng, Synergistic catalysis of AgPd@ZIF-8 on dehydrogenation of formic acid, Appl. Catal. B Environ. 165 (2015) 57–62. https://doi.org/10.1016/j.apcatb.2014.09.065.

[20] F. Sanchez, D. Motta, A. Roldan, C. Hammond, A. Villa, N. Dimitratos, Hydrogen Generation from Additive-Free Formic Acid Decomposition Under Mild Conditions by Pd/C: Experimental and DFT Studies, Top. Catal. (2018). https://doi.org/10.1007/s11244-018-0894-5.

[21] L. Prati, A. Villa, Gold colloids: From quasi-homogeneous to heterogeneous catalytic systems, Acc. Chem. Res. 47 (2014). https://doi.org/10.1021/ar400170j.

[22] F. Sanchez, M.H. Alotaibi, D. Motta, C.E. Chan-Thaw, A. Rakotomahevitra, T. Tabanelli, A. Roldan, C. Hammond, Q. He, T. Davies, A. Villa, N. Dimitratos, Hydrogen production from formic acid decomposition in the liquid phase using Pd nanoparticles supported on CNFs with different surface properties, Sustain. Energy Fuels. 2 (2018) 2705–2716. https://doi.org/10.1039/c8se00338f.

[23] S. Capelli, D. Motta, C. Evangelisti, N. Dimitratos, L. Prati, C. Pirola, A. Villa, Bio Adipic Acid Production from Sodium Muconate and Muconic Acid: A Comparison of two Systems, ChemCatChem. 11 (2019) 3075–3084. https://doi.org/10.1002/cctc.201900343.

[24] J.E. Matthiesen, J.M. Carraher, M. Vasiliu, D.A. Dixon, J.-P. Tessonnier, Electrochemical

Conversion of Muconic Acid to Biobased Diacid Monomers, ACS Sustain. Chem. Eng. 4 (2016) 3575–3585. https://doi.org/10.1021/acssuschemeng.6b00679.

[25] S. Campisi, D. Ferri, A. Villa, W. Wang, D. Wang, O. Kröcher, L. Prati, Selectivity Control in Palladium-Catalyzed Alcohol Oxidation through Selective Blocking of Active Sites, J. Phys. Chem. C. 120 (2016) 14027–14033. https://doi.org/10.1021/acs.jpcc.6b01549.

[26] H. Sakai, T. Nakajima, N. Yoshida, S. Kishimoto, Poisoning effect of carbon monoxide on the desorption process of hydrogen from palladium, React. Kinet. Catal. Lett. 19 (1982) 297–301. https://doi.org/10.1007/BF02074049.

[27] H. Noh, T.B. Flanagan, B. Cerundolo, A. Craft, Hydrogen-induced metal atom mobility in palladium-rhodium alloys, Scr. Metall. Mater. 25 (1991) 225–230. https://doi.org/10.1016/0956-716X(91)90385-E.

[28] C. Hu, J.K. Pulleri, S.W. Ting, K.Y. Chan, Activity of Pd/C for hydrogen generation in aqueous formic acid solution, Int. J. Hydrogen Energy. 39 (2014) 381–390. https://doi.org/10.1016/j.ijhydene.2013.10.067.

[29] Ö. Metin, X. Sun, S. Sun, Monodisperse gold-palladium alloy nanoparticles and their composition-controlled catalysis in formic acid dehydrogenation under mild conditions, Nanoscale. 5 (2013) 910–912. https://doi.org/10.1039/c2nr33637e.

[30] K. Tedsree, T. Li, S. Jones, C.W.A. Chan, K.M.K. Yu, P.A.J. Bagot, E.A. Marquis, G.D.W. Smith, S.C.E. Tsang, Hydrogen production from formic acid decomposition at room temperature using a Ag-Pd core-shell nanocatalyst, Nat. Nanotechnol. 6 (2011) 302–307. https://doi.org/10.1038/nnano.2011.42.

[31] S. Zhang, Ö. Metin, D. Su, S. Sun, Monodisperse AgPd Alloy Nanoparticles and Their Superior Catalysis for the Dehydrogenation of Formic Acid, Angew. Chemie Int. Ed. 52 (2013) 3681–3684. https://doi.org/10.1002/anie.201300276.

[32] A. Bulut, M. Yurderi, Y. Karatas, M. Zahmakiran, H. Kivrak, M. Gulcan, M. Kaya, Pd-MnOx nanoparticles dispersed on amine-grafted silica: Highly efficient nanocatalyst for hydrogen production from additive-free dehydrogenation of formic acid under mild conditions, Appl. Catal. B Environ. 164 (2015) 324–333. https://doi.org/10.1016/j.apcatb.2014.09.041.

[33] V. Mazumder, M. Chi, M.N. Mankin, Y. Liu, Ö. Metin, D. Sun, K.L. More, S. Sun, A Facile Synthesis of MPd (M = Co, Cu) Nanoparticles and Their Catalysis for Formic Acid Oxidation, Nano Lett. 12 (2012) 1102–1106. https://doi.org/10.1021/nl2045588.

[34] M. Yurderi, A. Bulut, M. Zahmakiran, M. Kaya, Carbon supported trimetallic PdNiAg nanoparticles as highly active, selective and reusable catalyst in the formic acid decomposition, Appl. Catal. B

Environ. 160–161 (2014) 514–524. https://doi.org/10.1016/j.apcatb.2014.06.004.

[35] K. Mori, H. Tanaka, M. Dojo, K. Yoshizawa, H. Yamashita, Synergic Catalysis of PdCu Alloy Nanoparticles within a Macroreticular Basic Resin for Hydrogen Production from Formic Acid, Chem. - A Eur. J. 21 (2015) 12085–12092. https://doi.org/10.1002/chem.201501760.

[36] X. Zhou, Y. Huang, W. Xing, C. Liu, J. Liao, T. Lu, High-quality hydrogen from the catalyzed decomposition of formic acid by Pd-Au/C and Pd-Ag/C, Chem. Commun. (2008) 3540–3542. https://doi.org/10.1039/b803661f.

[37] S. Capelli, A. Rosengart, A. Villa, A. Citterio, A. Di Michele, C.L. Bianchi, L. Prati, C. Pirola, Bio-adipic acid production by catalysed hydrogenation of muconic acid in mild operating conditions, Appl. Catal. B Environ. 218 (2017). https://doi.org/10.1016/j.apcatb.2017.06.060.

Support information

Figure S1. STEM image of monometallic Rh catalyst

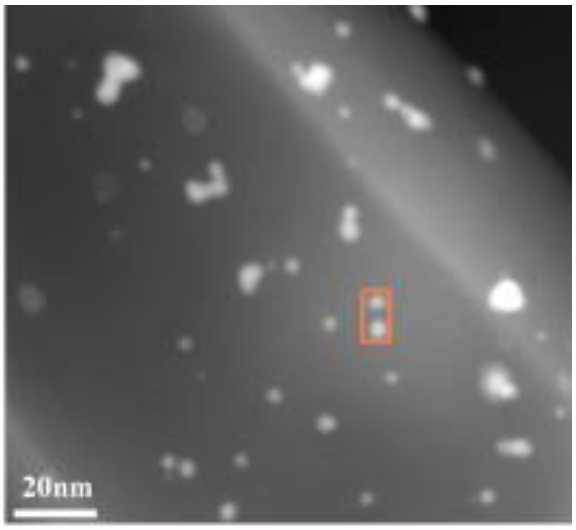

Figure S2 STEM images of Pd2Rh8 showing large aggregates of crystallites and b) STEM-XEDS analysis of a large aggregate ((Pd-Rh ratio: 1) 27:74, 2) 30:70)

a)

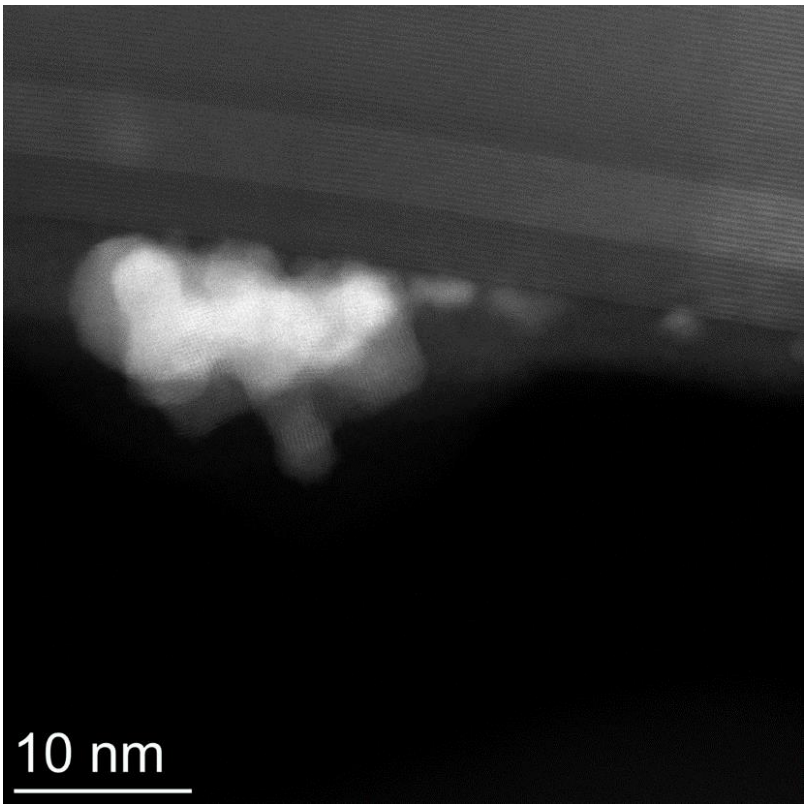

b)

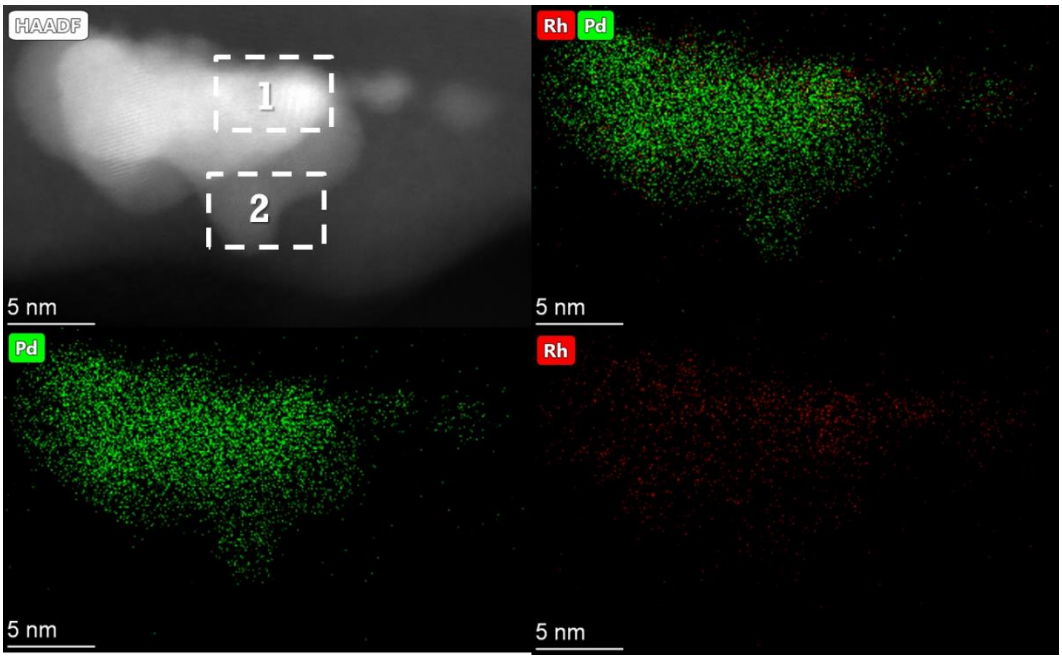

Figure S3 a) STEM images of Pd4Rh6 showing a large aggregation of particles and b) the corresponding EDX spectra showing an enrichment of Pd (Pd:Rh ratio of 79:21)

a)

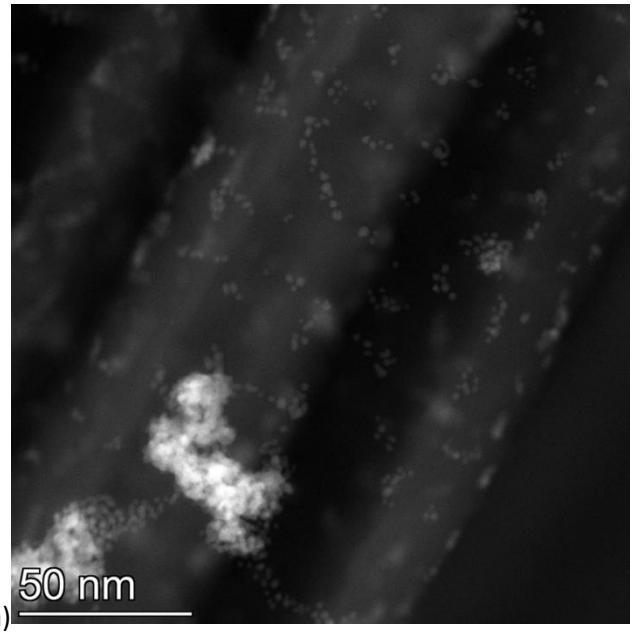

b) 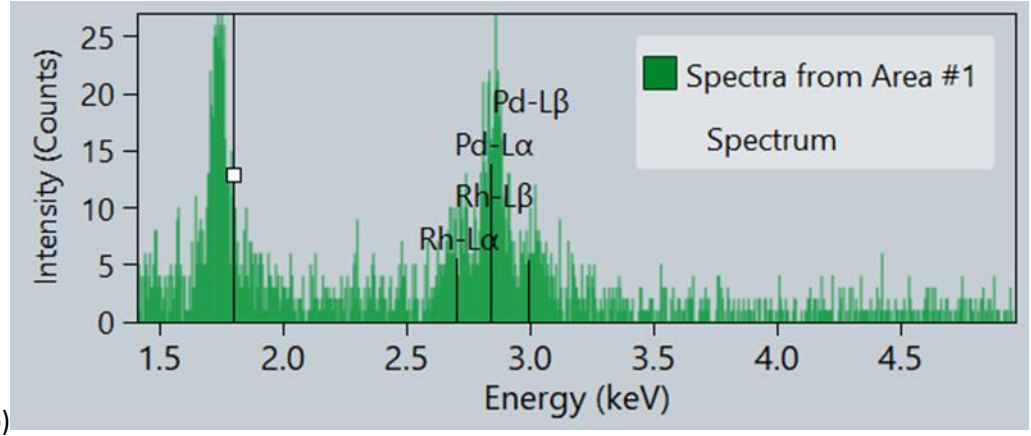

Figure S4 a) STEM images of Pd6Rh4 showing isolated large aggregation of particles